Oriented Electrostatic Effects on O_2 and CO_2 Reduction by a Polycationic Iron Porphyrin

Daniel J. Martin and James M. Mayer*

Department of Chemistry, Yale University, New Haven, Connecticut 06520-8107, United States
* james.mayer@yale.edu

Abstract

Next-generation energy technologies require improved methods for rapid and efficient chemical-to-electrical energy transformations. One new approach has been to include atomically-positioned, electrostatic motifs in molecular catalysts to stabilize high-energy, charged intermediates. For example, an iron porphyrin bearing four cationic, *ortho*-*N*,*N*,*N*-trimethylanilinium groups (*o*-$[N(CH_3)_3]^+$) has recently been used to catalyze the complex, multi-step O_2 and CO_2 reduction reactions (ORR and CO_2RR) with fast rates and at low overpotentials. The success of this catalyst is attributed, at least in part, to specific charge-charge interactions between the atomically-positioned *o*-$[N(CH_3)_3]^+$ groups and the bound substrate. However, by nature of the mono-*ortho* substitution pattern, there are four possible atropisomers of this metalloporphyrin and thus four unique electrostatic environments. This work reports that each of the four individual atropisomers catalyzes both the ORR and CO_2RR with fast rates and low overpotentials. The maximum turnover frequencies (TOF_{max}) vary among the atropisomers, by a factor of 60 for the ORR and a factor of 5 for CO_2RR. For the ORR, the αβαβ isomer is the fastest and has the highest overpotential, while for the CO_2RR, the order is reversed and the αααα isomer is the fastest and has the highest overpotential. The role of charge-positioning is complex and can affect more than a single step such as CO_2 binding. These data offer a first-of-a-kind perspective on atomically positioned charge and highlight the significance of *high charge density*, rather than orientation, on the thermodynamics and kinetics of multistep molecular electrochemical transformations.

Introduction

Electrostatic effects and electric fields are known to enable challenging reactions in biology, chemistry, and catalysis.[1-3] They are especially effective at facilitating reactions that involve charge redistribution or high-energy charged intermediates or transition states. Such reaction steps are common in molecular electrocatalysis, wherein multi-electron, multi-proton processes are often required for important chemical-to-electrical energy conversion reactions. To explore and utilize electrostatic effects, there has recently been a burgeoning interest in adding charged motifs to molecular (electro)catalysts.[4-12] The advantages of molecular catalysts in this context are that they can be designed with atomic precision and that they have well-defined active sites.

Perhaps the leading example of the value of adding charges to a catalyst is the polycationic iron porphyrin, Fe(*o*-TMA), which features four *ortho*-trimethylanilinium (*o*-$[N(CH_3)_3]^+$) groups on the porphyrin ligand. Under optimized conditions, this catalyst has been used to catalyze O_2 reduction and CO_2 reduction (ORR and CO_2RR) electrochemically with fast rates and at low overpotentials.[13-16] The success of Fe(*o*-TMA) towards both reactions has been ascribed, at least in part, to electrostatic interactions between the cationic groups on the porphyrin and ligands that bind to the metal center during turnover. In CO_2 reduction, the primary electrostatic interaction is hypothesized to be the stabilization of a high-energy $Fe^I(CO_2^{\bullet-})$ adduct using the well-positioned *o*-$[N(CH_3)_3]^+$ groups on the porphyrin ligand.[13,15,17] In O_2 reduction, electrostatic effects increase the binding affinity of Fe(*o*-TMA) towards acetate, the anionic conjugate base used to buffer the solution.[14-15] Acetate binding causes a subsequent change in the catalyst $E_{1/2}(Fe^{III}/Fe^{II})$, a property that controls O_2 binding and the rates of catalysis,[18-19] and thus ultimately defines the catalyst effectiveness.

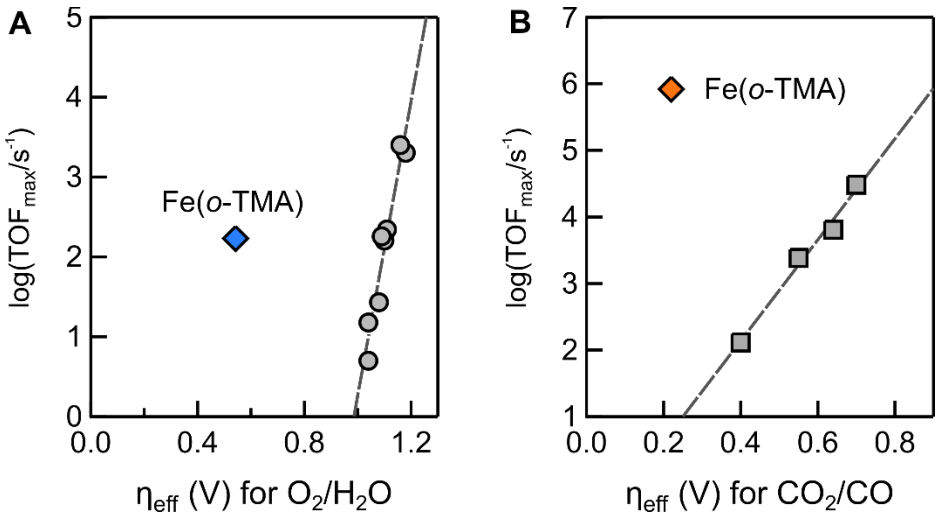

Figure 1. Maximum turnover frequency vs. effective overpotential plots, $\log(TOF_{max})/\eta_{eff}$, for (**A**) O_2 reduction and (**B**) CO_2 reduction by Fe(*o*-TMA) (colored data points) and neutral iron tetraarylporphyrin complexes (grey points). Data and details are from references 14 (**A**) and 13 (**B**). The $\log(TOF_{max})$ data in (**B**) are replotted here versus η_{eff} (the original data were plotted vs. $E°_{cat}$ (V vs. SHE)[13]); η_{eff} was determined by subtracting the reported $E°_{cat}$ values from the standard potential estimated in the Supporting Information of [13] ($E°_{CO2/CO}$ = -0.74 V vs. SHE).

Studies from the Savéant group and from our group have established Fe(*o*-TMA) among the leading soluble, molecular electrocatalysts for the CO_2RR and ORR, respectively (**Figure 1**). However, as was shown recently,[20] neither of these studies reported catalysis using genuine samples of the αβαβ atropisomer, as had been assumed. Rather—because a late-stage step in the reported synthesis involved heating and caused rotamerization of the αβαβ isomer—the reported catalysis in ref. 13 and 14 used a mixture of all four atropisomers (**Scheme 1**). Thus, it is not known which isomer(s) contribute most significantly to the catalytic prowess reported in the literature. We recently reported the synthesis and characterization of each of the atropisomers, which—once formed—are very stable to interconversion.[20] Therefore, this system is well-aligned to determine how the positioning of the cationic groups affects catalysis.

Scheme 1. Drawings of the four atropisomers of the $[Fe(o\text{-TMA})]^{5+}$ cation.

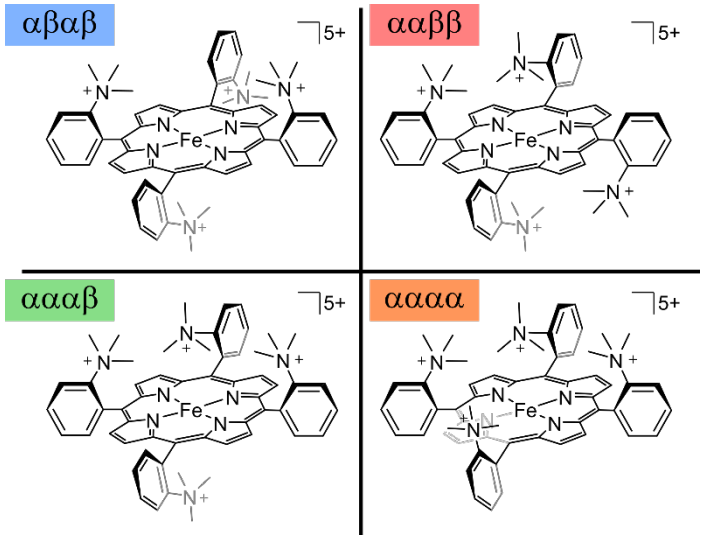

Here, we report electrocatalysis of the ORR and CO_2RR using each of the four individual atropisomers of Fe(*o*-TMA), and we identify the similarities and differences that exist between the isomers. Both kinetic and thermodynamic data suggest that the oriented, electrostatic groups in the Fe(*o*-TMA) ligand design have effects on multiple aspects of catalysis, beyond the stabilization of a single charged intermediate. From these comparisons, the most important electrostatic factors were identified and detailed for catalysis of both reactions. The results and conclusions of this work have important implications for the design of molecular (electro)catalysts with atomically positioned charged groups.

Results and Discussion

The presentation below is divided into two main sections. **Section I** presents the electrocatalysis of the ORR by the different Fe(*o*-TMA) isomers, which occurs at the Fe(III/II) redox couple. Since the Fe(III/II) redox couple, and thus ORR catalysis, is strongly modulated by the ligation of acetate,[14,15] we also report the equilibrium constants, enthalpy, and entropy of acetate binding in this section. **Section II** presents the CO_2RR by Fe(*o*-TMA), which occurs at the Fe(I/0) redox couple, where ligand binding does not play a role. Under such conditions, the unusual catalytic waves have implications about the mechanism of CO_2 reduction and the overpotential at which catalysis occurs.

Experimental Overview

The four atropisomers of iron(III) tetra(*N*,*N*,*N*-trimethylanilinium)porphyrin pentatriflate and the ferrous (Fe^{II}) tetratriflate salts were prepared as previously reported.[15,20] Cyclic voltammograms (CVs) were collected in acetonitrile (MeCN) or *N*,*N*-dimethylformamide (DMF) solutions containing 0.1 M tetra-*n*-butylammonium hexafluorophosphate ([*n*-Bu_4N][PF_6]), as noted, and were referenced versus ferrocene (Fc^+/Fc). The unique solution conditions for specific experiments are given below and in the Supporting Information (SI).

CVs of the four atropisomers, first reported in reference [20], show three reversible redox features in both MeCN and DMF, under argon, formally the iron(III/II), iron(II/I), and iron(I/0) redox couples. The $E_{1/2}$ values for each of the couples are significantly positive of typical values reported for neutral iron tetraarylporphyrins (see **Table 1** and reference [20]). The different atropisomers have very similar reduction potentials, showing that the through-space orientation of the charged groups does not significantly affect the reduction thermodynamics. It is important, however, that the substituents are *ortho* to the porphyrin, as these atropisomers have $E_{1/2}$ values that are 0.1-0.2 V more positive than that for the corresponding *para*-$[N(CH_3)_3]^+$ substituted complex, Fe(*p*-TMA), in each respective solvent.[20] As described below, the voltammetry data under *catalytic conditions* is more varied for the set of Fe(*o*-TMA) atropisomers.

I. O_2 Reduction

A) ORR catalysis

The electrocatalysis of oxygen reduction by each of the four atropisomers was examined under the solution conditions that gave the best catalysis for the mixture of isomers in ref 14: MeCN containing 0.1 M H_2O, 1:1 buffered acetic acid/acetate (AcOH/AcO^-), and 0.1 M [*n*-Bu_4N][PF_6]. Under these conditions, one acetate is bound to the iron porphyrin complex in both the ferrous and ferric states and acetic acid is the proton donor.[14-15] Acetate must also be bound in the Fe^{III}-superoxide complex since no O_2 binding is observed in the absence of a coordinating ligand.[15] A single stock solution with these components was prepared and divided into four separate containers, to each of which was added one of the Fe(*o*-TMA) isomers. This method ensured that the isomers were compared under *identical* solution conditions and that the equilibrium potential for O_2 reduction was constant across the series (see SI). Cyclic voltammograms were measured for each of these solutions under both argon and O_2 (1 atm) (**Figures S1, S2**).

In the presence of AcOH/AcO$^-$ buffer, all four isomers have reversible iron(III/II) redox features under argon, with $E_{1/2}(Fe^{III}/Fe^{II})$ values between −0.595 V (αααα) and −0.644 V (αβαβ). Under O_2, a large, irreversible current appeared near the corresponding $E_{1/2}(Fe^{III}/Fe^{II})$ values, indicating turnover (**Figure 2A**). Rinse tests indicated that this current was the result of a homogeneous catalytic process (**Figure S3**).[21-22] In all cases the catalytic voltammograms were far from ideal. The catalytic current all began at potentials positive of the corresponding $E_{1/2}$ values for all four atropisomers, as expected. At potentials more that were 0.1-0.2 V more negative than the catalyst $E_{1/2}$ values, the currents increased more steeply. The origin of this deviation from ideality at potentials more negative than the catalyst $E_{1/2}$ values is not evident, and we restrict our analysis here to the foot of the wave, the region in the dotted box in **Figure 2A**. As we have done in prior papers analyzing the ORR by iron porphyrin electrocatalysts,[14,19,22] the Savéant foot-of-the-wave analysis (FOWA) was used to determine the maximum catalytic turnover frequencies (TOF_{max}) values corresponding to this region of these voltammograms. This foot of the catalytic waves has the advantage that unwanted side-phenomena such as substrate depletion are minimized (**Figure 2B** and **Figure 2C**; see SI for details).[23-24] The effective thermodynamic overpotential at which these catalysts operate (η_{eff}) was determined from the $E_{1/2}(Fe^{III}/Fe^{II})$ and the solution conditions.[14,16] **Table 1** gives these values for the different isomers under identical conditions.

Table 1. Catalyst system properties for O_2 reduction by Fe(*o*-TMA) atropisomers.[a]

Atropisomer	$E_{1/2}(Fe^{III}/Fe^{II})$		$\Delta E_{1/2}$ (V)[b]	η_{eff} (V)[c]	TOF_{max} (s^{-1})[d]	$\log(TOF_{max}/s^{-1})$
	–	+ 0.1 M AcOH buffer				
αβαβ	0.142	−0.644	–0.786	0.491	60	1.8
ααββ	0.143	−0.626	–0.769	0.474	7	0.8
αααβ	0.130	−0.611	–0.741	0.458	6	0.8
αααα	0.135	−0.595	–0.730	0.442	1	0

[a] All experiments used O_2-saturated (1 atm) solutions of MeCN containing 0.2 mM Fe(*o*-TMA) 0.1 M acetic acid buffer (1:1 AcOH/AcO$^-$), 0.1 M H_2O, and 0.1 M [*n*-Bu_4N][PF_6], except for the 2nd column which gives the $E_{1/2}$ values in the absence of O_2 and buffer (from ref. [15]). [b] Shift in the Fe(III/II) couple upon addition of AcOH/AcO$^-$ buffer. [c] Effective overpotential for ORR catalysis. [d] Maximum ORR turnover frequency from FOWA analysis. Uncertainties in TOF_{max} are ca. ±15%.

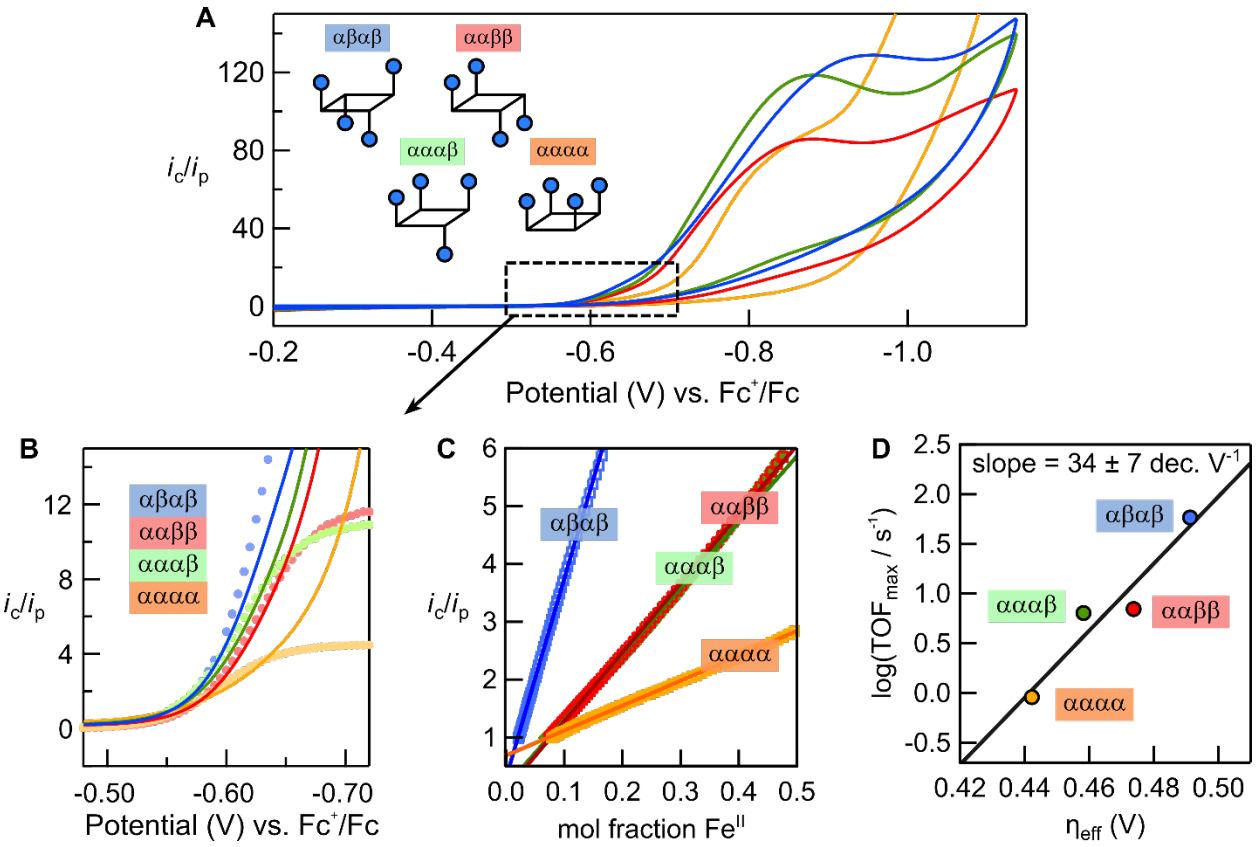

Figure 2. Electrochemical O_2 reduction by Fe(*o*-TMA) atropisomers. (**A**) Cyclic voltammograms for O_2 reduction by the Fe(*o*-TMA) isomers. The atropisomers are shown as ball and stick models for clarity, and the region fit by FOWA is shown with a dotted black box. (**B**) Same data as indicated in (**A**), as well as simulated curves for the corresponding $E_{1/2}$ and TOF_{max} values reported in **Table 1**. (**C**) FOWA plots, showing fits to the linear region (see SI). (**D**) Plot of $\log(TOF_{max})$ versus η_{eff} for the data shown in (**B,C**) with linear fit. Conditions and results from **Table 1**.

All four isomers of Fe(*o*-TMA) catalyze O_2 reduction with fast rates and at low overpotentials under these conditions. Their TOF_{max} range from 1−60 s^{-1} and η_{eff} from 0.44−0.49 V. The αβαβ isomer is the fastest of the series and the αααα isomer is the slowest, with the ααββ and αααβ isomers having TOF_{max} that are in between. The four atropisomers show a roughly linear relationship between $\log(TOF_{max})$ and $E_{1/2}(Fe^{III}/Fe^{II})$—and thus η_{eff}—with a slope of 34 ± 7 decades V^{-1} (**Figure 2D**).

The mechanism for O_2 reduction by both iron tetraphenylporphyrin and the atropisomeric mixture of Fe(*o*-TMA) catalysts is known in nonaqueous solvents.[18,25] Catalysis involves *i*) the initial reduction of the ferric porphyrin ($[Fe^{III}(P)]^+$) to the ferrous form ($Fe^{II}(P)$), *ii*) rapid O_2-binding to form the corresponding ferric superoxide complex ($Fe^{III}(P)(O_2^{\bullet-})$) and *iii*) rate-limiting proton transfer by exogenous acid (AcOH under these conditions) to form $[Fe^{III}(P)(O_2H^{\bullet})]^+$. An additional $3e^-/3H^+$ are added in rapid follow-up steps to complete turnover (see references [18] and [25] for complete details). From this mechanistic insight, we have previously identified linear relationships that exist between $\log(TOF_{max})$ and $E_{1/2}(Fe^{III}/Fe^{II})$ for simple iron porphyrin systems.[18] These relationships are directly related to the dependence of O_2 binding and the barrier for proton transfer on the catalyst $E_{1/2}(Fe^{III}/Fe^{II})$, both of which are steps that impact the reaction kinetics.

In general, catalysts with more negative $E_{1/2}(Fe^{III}/Fe^{II})$ values are more nucleophilic, bind O_2 more strongly, and result in more basic iron superoxide intermediates, all of which increase reaction rates.

What is striking about the $\log(TOF_{max})$ vs. $E_{1/2}$ relationship for the Fe(*o*-TMA) atropisomers is that it is almost two times steeper than the previously reported slope for neutral iron porphyrin catalysts, even considering the large standard deviation. Given that the rate law is unchanged (see ref. [14]), the steeper slope indicates a more sensitive relationship between $E_{1/2}$ and (*i*) the free energy of O_2-binding ($\Delta G_{O2} = -RT\ln K_{O2}$), (*ii*) the distal O-atom basicity of the corresponding ferric superoxide complexes ($pK_a[O_d]$) and/or (*iii*) the kinetic Brønsted α for protonation of the superoxide. Previous computational data on the rotamers of bound O_2 suggests that there is little-to-no stabilization effect of bound superoxide by the charged *o*-$[N(CH_3)_3]^+$ groups, at least for the αβαβ atropisomer.[15] While differences in dioxygen binding to the different atropisomers cannot be ruled out, it seems likely that thermochemistry and barrier for proton transfer are the parameters that are most sensitive to the atropisomer identity and $E_{1/2}$ value. The proton transfer involves the formation of an *anionic* acetate molecule adjacent to the polycationic porphyrin and is therefore most likely to be affected by the positioning of the cationic groups. These topics will be explored in future work.

Simply identifying the *existence* of a linear relationship between $\log(TOF_{max})$ and $E_{1/2}(Fe^{III}/Fe^{II})$ is valuable, because it indicates that differences in catalytic efficacy within the Fe(*o*-TMA) atropisomers is—at least in part—due to differences in the atropisomer $E_{1/2}(Fe^{III}/Fe^{II})$ values.

B) Acetate binding

In MeCN containing only supporting electrolyte, the Fe(*o*-TMA) atropisomers have $E_{1/2}(Fe^{III}/Fe^{II})$ values that range between 0.130 and 0.143 V vs. Fc^+/Fc. In solutions containing 0.1 M buffered AcOH, acetate binding causes the $E_{1/2}(Fe^{III}/Fe^{II})$ values to shift to dramatically more negative potentials, between −0.595 and −0.644 V vs. Fc^+/Fc (**Table 1**). The magnitude of the shift is remarkable, ca. *–0.75 V* for the αβαβ isomer, and necessary for generating a sufficiently nucleophilic metal center to bind O_2 and rapidly turn over.[15]

The shift in $E_{1/2}(Fe^{III}/Fe^{II})$ that accompanies acetate binding ($\Delta E_{1/2}$) reflects the difference in acetate binding constants to the iron(III) and iron(II) oxidation states—$K_{AcO}(Fe^{III})$ and $K_{AcO}(Fe^{II})$—for each of the respective atropisomers.[15] This is a result of Hess' Law, which relates the binding constants and $E_{1/2}(Fe^{III}/Fe^{II})$ values by their respective difference in free energies (**Scheme 2** and **eq 1**). The large, negative shift in $E_{1/2}(Fe^{III}/Fe^{II})$ indicates that $K_{AcO}(Fe^{III}) >> K_{AcO}(Fe^{II})$ for all four isomers, by 12 or 13 orders of magnitude. This analysis gives the *ratio* of the $K_{AcO}(Fe^{III})$ and $K_{AcO}(Fe^{II})$ for each isomer, but it does not yield either of the separate binding constants.

Scheme 2. Square scheme for relating acetate binding constants and $E_{1/2}$ values. Reproduced from ref. [15].

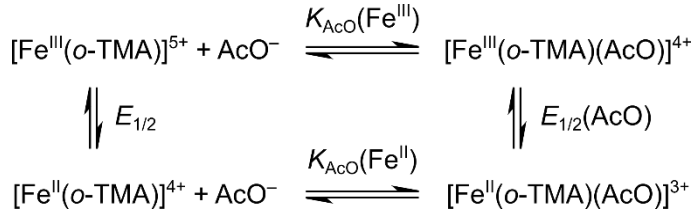

$$E_{1/2} - E_{1/2}(\mathrm{AcO}) = (2.303RT)\left\{\log(K_{\mathrm{AcO}}(\mathrm{Fe^{III}})) - \log(K_{\mathrm{AcO}}(\mathrm{Fe^{II}}))\right\} \quad (\mathbf{1})$$

The changes in $E_{1/2}$ upon acetate binding ($\Delta E_{1/2}$) are different for each atropisomer (**Table 1**). As a result, the ratio of $K_{AcO}(Fe^{III})$ and $K_{AcO}(Fe^{II})$ is also unique to each atropisomer. These unique ratios of

$K_{AcO}(Fe^{III})/K_{AcO}(Fe^{II})$ is one of the primary reasons that the atropisomers have different $E_{1/2}(Fe^{III}/Fe^{II})$ values under electrocatalytic conditions. The reason that the αβαβ isomer has the most negative $E_{1/2}(Fe^{III}/Fe^{II})$ is because the difference between $K_{AcO}(Fe^{III})$ and $K_{AcO}(Fe^{II})$ is largest for this atropisomer. Likewise, the αααα isomer has the most positive $E_{1/2}(Fe^{III}/Fe^{II})$ because the difference in binding constants to Fe^{III} and Fe^{II} is smallest (*i.e.*, they are most similar).

To better understand these differences, acetate binding was measured to both the ferric and ferrous forms of the Fe(*o*-TMA) atropisomers. The ferrous binding constants $K_{AcO}(Fe^{II})$ were measured by UV-visible spectroscopy. The addition of *n*-tetrabutylammonium acetate, [*n*-Bu_4N][AcO], to pink solutions of the $[Fe^{II}(o\text{-TMA})]^{4+}$ isomers resulted in a color change and the formation of a new, green species (**Figure S6-Figure S9**). The 1:1 stoichiometry of this reaction and the binding constant at 20 °C have already been reported for the αβαβ.[15] The optical spectra for each $[Fe^{II}(o\text{-TMA})]^{3+}$ and $[Fe^{II}(o\text{-TMA})(AcO)]^{3+}$ were not affected by the identity of the atropisomer, respectively, and so the acetate-to-porphyrin stoichiometry was also assumed to be 1:1 for the other isomers (**Figure S1—Figure S11**).

$$K_{AcO}(M^{-1}) = \frac{\left[[Fe^{II}(P)(AcO)]^{n-1}\right]}{\left[[Fe^{II}(P)]^{n}\right]\left[AcO^{-}\right]} \quad (2)$$

Equilibrium constants for acetate binding to each $[Fe^{II}(o\text{-TMA})]^{4+}$ atropisomer (**eq 2**) were measured by variable temperature UV-vis spectroscopy. For each isomer, a solution containing ~35 μM $[Fe^{II}(o\text{-TMA})]^{4+}$, 0.1 mM [*n*-$Bu_4N$][AcO], and 0.1 M [*n*-$Bu_4N$][$PF_6$] was temperature equilibrated between −40 °C and 40 °C with regular spectra being collected (**Figure S12-Figure S15**). The UV-vis spectra were fit to linear combinations of the genuine $[Fe^{II}(o\text{-TMA})]^{4+}$ and $[Fe^{II}(o\text{-TMA})(AcO)]^{3+}$ spectra, following the fitting methods reported in reference [20]. The 0.1 M supporting electrolyte was added to match electrochemical conditions and to minimize differences in ionic strength between samples. A van ′t Hoff analysis was used to probe the enthalpy and entropy components of acetate binding to the ferrous complexes (**Figure 3**). The ferric binding constants ($K_{AcO}(Fe^{III})$) were determined using **eq 1** with the experimental $K_{AcO}(Fe^{II})$ and $\Delta E_{1/2}$ values (**Table 1**). The pertinent binding constants, free energies, enthalpies, and entropies are summarized in **Table 2**. All other binding constants are reported in the Supporting Information (**Table S1**).

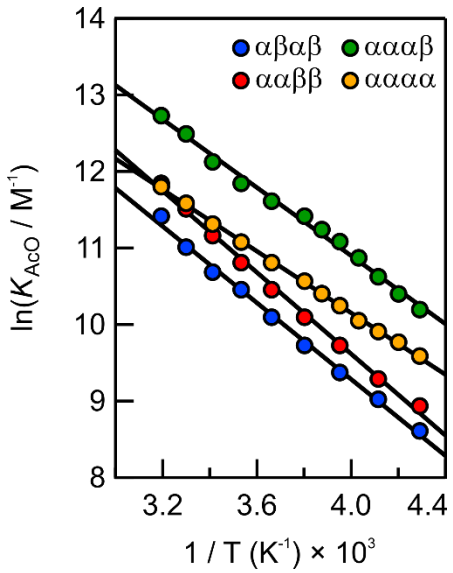

Figure 3. van ′t Hoff plots for acetate binding to the $[Fe^{II}(o\text{-TMA})]^{4+}$ isomers in MeCN containing 0.1 M [*n*-Bu_4N][PF_6]. Thermochemical parameters summarized in **Table 2**.

Table 2. Thermochemical parameters for acetate binding to Fe(*o*-TMA) atropisomers [a]

Reaction and Atropisomer	$\Delta H°$ [b] (kcal mol^{-1})	$\Delta S°$ [c] (cal mol^{-1} K^{-1})	ΔG [d] (kcal mol^{-1})	log(K_{AcO}/M^{-1}) [e]
$[Fe^{II}(o\text{-TMA})]^{4+} + AcO^- \rightleftharpoons [Fe^{II}(o\text{-TMA})(AcO)]^{3+}$				
αβαβ	5.0	38	−6.3 [f]	4.7 [f]
ααββ	5.3	40	−6.5	4.8
αααβ	4.4	39	−7.1	5.3
αααα	4.0	36	−6.6	4.9
$[Fe^{III}(o\text{-TMA})]^{5+} + AcO^- \rightleftharpoons [Fe^{III}(o\text{-TMA})(AcO)]^{4+}$			ΔG [g] (kcal mol^{-1})	log(K_{AcO}/M^{-1}) [e]
αβαβ	–	–	−24.3	18.0
ααββ	–	–	−24.1	17.8
αααβ	–	–	−24.1	17.9
αααα	–	–	−23.3	17.3

[a] MeCN solutions containing 0.1 M [*n*-Bu$_4$N][PF$_6$]. [b] Uncertainties are ± 0.1 kcal mol^{-1}. [c] Uncertainties are ± 2 cal mol^{-1} K^{-1}. [d] Calculated from $\Delta H°$ and $\Delta S°$ at 20 °C, the temperature at which the electrochemistry was performed. Uncertainties are ± 0.3 kcal mol^{-1}. [e] Uncertainties are ± 0.2 units. [f] The value reported in reference [20] is −6.5 kcal mol^{-1}, which was determined using a single temperature measurement. The two values are within error of one another. [g] Estimated using eq 1 and ΔG values for acetate binding to $[Fe^{II}(o\text{-TMA})]^{4+}$ at 20 °C. Uncertainties are ± 0.3 kcal mol^{-1}.

In all cases, the van ′t Hoff parameters reveal that the free energies of acetate binding to the ferrous forms are dominated by large, positive entropy terms (average $\Delta S°(Fe^{II}) = 38 \pm 2$), while the enthalpies of binding are unfavorable. The large and positive entropy terms were initially surprising, especially given that the forward equilibrium is bimolecular. However, the solvation of highly charged ions organizes a substantial number of solvent molecules and electrolyte ions.[26] Binding of acetate lowers the charge and releases some of these organized species.

The free energies for acetate binding to $[Fe^{II}(o\text{-TMA})]^{4+}$ are significant at 20 °C, with $\Delta G(Fe^{II})$ = −6.3 to −7.1 kcal mol^{-1}. The corresponding energies for acetate binding to $[Fe^{III}(o\text{-TMA})]^{5+}$ are much more negative, $\Delta G(Fe^{III})$ = −24.3 to −23.3 kcal mol^{-1}. A similar result was previously reported for the αβαβ isomer of Fe(*o*-TMA) in *n*-butyronitrile.[15] An increase in binding constants to the ferric porphyrin was expected due to the higher charge of the pentacationic $[Fe^{III}(o\text{-TMA})]^{5+}$ complex and higher affinity for ligands in general, but the increase of ~10^{13} seems remarkable.

There is no clear relationship between the free energies of acetate binding and the orientations of the charges in the different atropisomers, in either the ferrous or ferric forms. The $\Delta G(Fe^{II})$ values trend slightly more negative with increasing charge density on a given face, but the $\Delta G(Fe^{III})$ values do not. The αααα isomer is unusual because it does not conform to either trend. For instance, acetate binding to the ferrous αααα isomer is less favorable than binding to the αααβ form, despite the increased charge density on the α-face. Likewise, acetate binding is weakest to the ferric αααα isomer, more so than to any of the other atropisomers. While the origins of these deviations are unknown, it is possible that the highly-charged α-face may be competitively binding OTf^- or PF_6^- anions. This hypothesis is consistent with crystallographic data reported in reference [20], which showed a triflate ligand bound to the αααα atropisomer in both ferric and ferrous solids. While the other ferric atropisomer structures showed a bound triflate, only the αααα had a bound anion in the ferrous form. In both the Fe^{III} and Fe^{II} oxidation states, the triflate ligand was bound to the more crowded, more cationic α-face. Assuming a similar interaction exists in the solution state, the enhanced interaction with supporting anions may decrease the favorability of acetate binding

measured in this work. It could also be that the differences are dominated by disparities in solvation entropies since a 5+ ion will organize many solvent molecules and counterions in its vicinity.

These thermochemical data indicate that the *orientation* of the *o*-$[N(CH_3)_3]^+$ groups does not affect $\Delta S°(Fe^{II})$ and only subtly affects $\Delta H°(Fe^{II})$ for acetate binding. Rather, the *net* change in charge upon ligand binding is far more important than the through-space position of the charges. This is an important result in general, and specifically for ORR by these complexes, because these thermochemical parameters control acetate binding and thus the catalyst $E_{1/2}(Fe^{III}/Fe^{II})$.

C) ORR Conclusions

All four atropisomers of Fe(*o*-TMA) operate with high turnover frequencies and low overpotentials for O_2 reduction in MeCN containing buffered acetic acid. The four are quite similar in their properties: the $E_{1/2}(Fe^{III}/Fe^{II})$ values differ by less than 50 mV—with and without an acetate ligand—and the acetate binding constants vary only by a factor of 5 among the isomers, for both the Fe^{II} and Fe^{III} complexes. The catalytic rate constants (proportional to TOF_{max}) vary by a factor of 60, with the αβαβ isomer being the most reactive.

The most important factor controlling the relative values of both TOF_{max} and η_{eff} for these systems is the catalyst $E_{1/2}(Fe^{III}/Fe^{II})$ under electrocatalytic conditions. While this is a common situation for molecular electrocatalysts, there is an unusual origin of the $E_{1/2}$ differences in this case. From electrochemical data and van ′t Hoff plots of optical data, the $E_{1/2}(Fe^{III}/Fe^{II})$ values under catalytic conditions were shown to depend on the *difference* in acetate binding thermodynamics to the ferric and ferrous forms of Fe(*o*-TMA) (**Figure 4**, right). The $E_{1/2}(Fe^{III}/Fe^{II})$—and therefore TOF_{max} values—do *not* correlate with the acetate binding constant to the active, ferrous form of the catalyst (**Figure 4**, left). For instance, acetate binding is least favorable to the ferrous αβαβ isomer, yet the same isomer has the most negative $E_{1/2}(Fe^{III}/Fe^{II})$ and fastest TOF_{max} (**Figure 4**). This shows that even a simple model—that ligand-binding generates the active catalyst—depends on several parameters in different oxidation states.

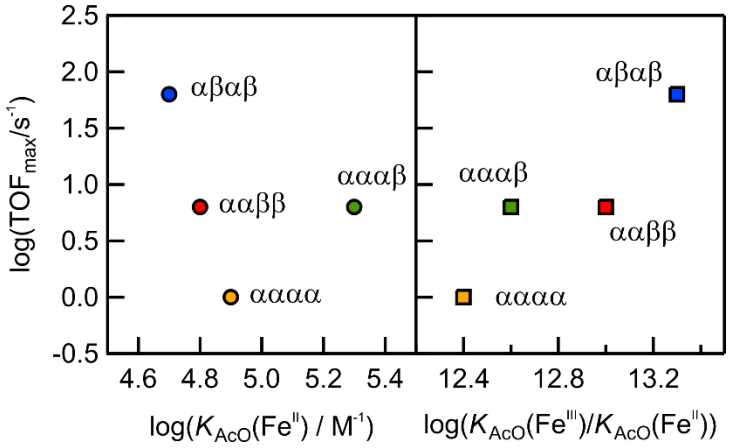

Figure 4. The values of $\log(TOF_{max})$ for the various atropisomers vs. (left) the ferrous acetate binding constants and (right) the *difference* between the ferric and ferrous binding constants. Only the right plot shows a roughly linear trend.

The *slope* of the $\log(TOF_{max})/E_{1/2}$ relationship for the Fe(*o*-TMA) atropisomers is nearly twice as steep as the $E_{1/2}$ relationship previously reported for a series of substituted iron tetraarylporphyrin catalysts.[17] The steeper slope indicates a more sensitive relationship between the catalyst $E_{1/2}(Fe^{III}/Fe^{II})$, the dioxygen binding constant, the basicity of the corresponding superoxide intermediates, and/or the barrier to superoxide protonation. It is clear that the effects of the positioned cationic charges are multiple rather than being concentrated in one specific step of the catalytic cycle.

II. CO_2 Reduction

A) Catalytic rates for the different atropisomers

Fe(*o*-TMA), as a mixture of the four atropisomers, is among the leading molecular catalysts for CO_2 electroreduction.[13] With the four isolated isomers in hand, we set out to determine their relative activity, and the effects of the positioned cations. As an added benefit, the results provide an indirect test of the hypothesis by Savéant *et al*. that the success of this catalyst is due, at least in part, to the stabilization of a high energy $Fe^{I}(CO_2^{\bullet-})$ intermediate by the well-positioned *o*-$[N(CH_3)_3]^+$ groups in the αβαβ atropisomer. Computational studies support stabilization of the $CO_2^{\bullet-}$ ligand when its partially anionic oxygens are near the cations of the αβαβ isomer;[15,17] however, no direct experimental or computational evidence connects this proposed stabilization with improved catalysis.

In order to match the electrochemical conditions reported in ref. 13, a DMF solution was prepared to contain 0.1 M [*n*-Bu_4N][PF_6], 0.1 M H_2O, and 3.0 M PhOH (note that this is perhaps better described as electrolyte and water in a mixed solvent of ~0.76 mole fraction DMF and ~0.24 mole fraction phenol). This single solution was divided into four containers before dissolving each of the respective atropisomers. CVs were collected for each of the four solutions under both argon and 1 atm CO_2 (**Figure S17-Figure S18)**. The CVs were corrected for internal resistance following the method of Dempsey et al.[27] Some error in (over)potentials was likely introduced as a result of this correction; however, we emphasize that the discussion and interpretation of the data below relies only on the relative reactivity of the atropisomers.

Under Ar, the formal iron(I/0) redox couple is almost unaffected by the atropisomer identity, with an average $E_{1/2}(Fe^{I}/Fe^{0}) = -1.695 \pm 0.006$ V (**Table 3**; called the "formal" Fe^{I}/Fe^{0} couple because the possible redox non-innocence of the porphyrin ligand complicates the oxidation state assignments). Under 1 atm of CO_2, a large, irreversible current appeared, obscuring the iron(I/0) couple for each solution. The irreversible, cathodic current is indicative of catalysis and is consistent with data previously reported by the Savéant group.[13] A loss of reversibility in the iron(II/I) redox feature and formation of a new anodic peak at more negative potentials indicates that CO is a significant product formed during turnover (**Figure 5**; arrow).[28-29]

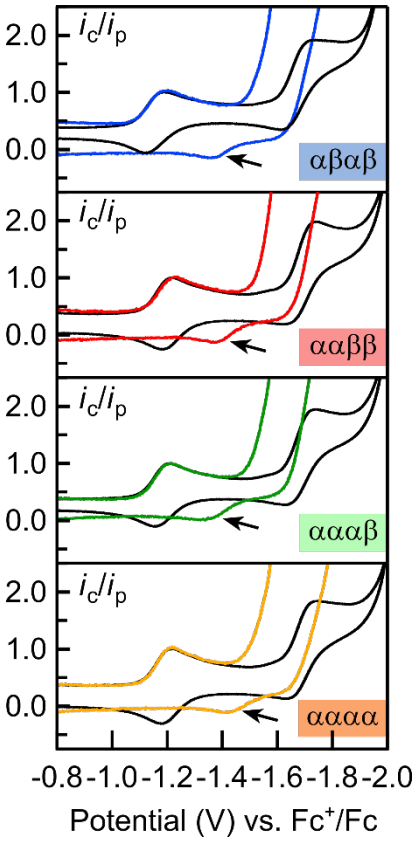

Figure 5. Cyclic voltammograms of Fe(*o*-TMA) atropisomers under 1.0 atm Ar (black traces) and CO_2 (colored traces), showing region containing Fe^{II}/Fe^{I} and Fe^{I}/Fe^{0} redox features. The arrow in each panel implicates the formation of carbon monoxide as the product, which forms a carbonyl complex during the anodic sweep.[28-31] All data were collected at 0.1 V s^{-1} in DMF containing 3.0 M PhOH, 0.1 M H_2O, and 0.1 M [*n*-Bu_4N][PF_6]. Data shown are normalized to the non-catalytic peak current of the Fe^{II}/Fe^{I} redox couple, which is constant under both Ar and CO_2.

Following the methodology reported by Savéant *et al.*, the TOF_{max} values for CO_2-to-CO reduction were derived from currents obtained at fast scan rates.[13,28-29,32] At moderate scan rates (0.1 V s^{-1}), the current-potential responses were peak-like, indicating the presence of confounding factors such as substrate depletion, product inhibition, or other phenomena. For several of the atropisomers a second peak was observed at more cathodic potentials than the first, indicating that a second mechanistic pathway likely occurs under conditions of reagent depletion. Raising the scan rate decreased the significance of these unwanted side processes and led to more canonical S-shaped voltammograms. At fast scan rates (>100 V s^{-1}), the plateau currents saturated and ultimately reached scan rate-independent values (i_{pl}). Under these limiting conditions, **eq 3** can be used to derive TOF_{max} using only the i_{pl}/i_p, , v (0.1 V s^{-1} for the i_p CV), and the constants R, T, and F.[13] The derivation of **eq 3** for the mechanism described below is available in the Supporting Information.

$$\frac{i_{pl}}{i_p} \approx 4.48\sqrt{\frac{\mathrm{TOF_{max}}RT}{vF}} \qquad (3)$$

All four atropisomers reach large, current-limiting plateaus at fast scan rates (**Figure 6**). While the normalized plateau currents (i_{pl}/i_p) are different by inspection, the corresponding TOF_{max} values are quite similar (**Table 3**). The log(TOF_{max}) values range from 4.6 for the αβαβ atropisomer to 5.3 for the αααα.

These values are near the estimated upper-limit [log(TOF_{max}) < 6] previously reported in reference 13, and are summarized in **Table 3**.

Table 3. Catalyst system properties for CO_2 reduction by Fe(*o*-TMA) atropisomers.[a]

Atropisomer	$E_{1/2}(Fe^{II/I})$[a]	$E_{1/2}(Fe^{I/0})$[b]	$E_{Q'/B}$ (V)[c]	η_{eff} (V)[d]	TOF_{max} (s^{-1})[e]	log(TOF_{max}/s^{-1})
αβαβ	−1.157	−1.691	−1.82	0.39	4×10^4	4.6
ααββ	−1.199	−1.705	−1.82	0.39	1×10^5	5.0
αααβ	−1.183	−1.693	−1.80	0.37	1×10^5	5.0
αααα	−1.196	−1.694	−1.90	0.48	2×10^5	5.3

[a] In DMF solutions containing 3.0 M PhOH, 0.1 M H_2O, 0.1 M [*n*-Bu_4N][PF_6] and 1 atm CO_2. [b] Same conditions as a except without CO_2. [c] $E_{Q'/B}$ defined for 3.0 M PhOH, 1.0 atm CO_2, and 0.1 M H_2O under turnover conditions (see text). [d] Values recalculated from ref [13] by subtracting $E_{Q'/B}$ from the equilibrium potential for CO_2/CO reduction from [13] (E_{CO2RR} = −1.43 V vs. Fc^+/Fc), see text. [e] Uncertainties are ±15%.

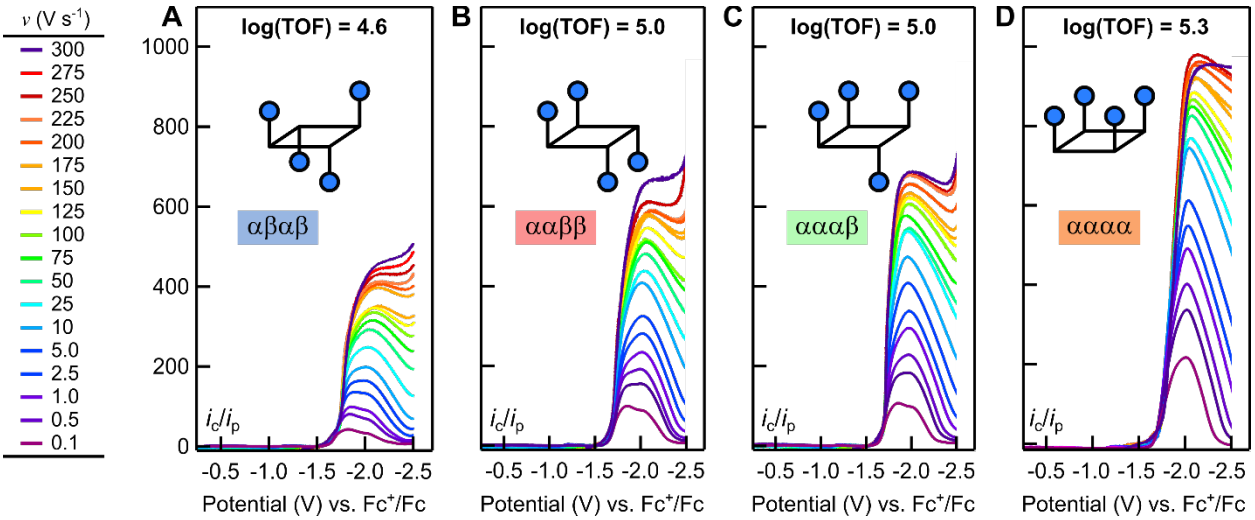

Figure 6. Linear sweep voltammograms for CO_2 reduction at various scan rates, showing an approach to the canonical S-shaped current-potential response for the (**A**) αβαβ, (**B**) ααββ, (**C**) αααβ, and (**D**) αααα isomers of Fe(*o*-TMA). Data were collected as cyclic voltammograms but the reverse scan is not shown (see SI). Data were corrected for internal resistance and capacitive currents before being normalized to i_p (collected at 0.1 V s^{-1}). See Supporting Information for raw data and complete details.

These results are impactful for two reasons. First, all four atropisomers are exceptional catalysts for CO_2 reduction and achieve some of the fastest rates in the homogeneous electrochemistry literature. Second, and perhaps more striking, the maximum difference in rates for the four electrostatic isomers is only a factor of 5. The similarity in rates is surprising and shows that *the orientation of the o-$[N(CH_3)_3]^+$ groups does not substantially affect the reaction kinetics*. Rather, *only the existence of the o-$[N(CH_3)_3]^+$ groups in the porphyrin design is important*. This is in spite of the fact that the αααα isomer should generate a significant electric field along its C_4 axis, while the D_{2d} αβαβ isomer has higher symmetry and no net dipole moment. It is noteworthy that the corresponding *p*-$[N(CH_3)_3]^+$ isomer has much slower rates than any of the *ortho*-substituted atropisomers under these conditions.[13,20]

These results do not support any large kinetic benefit of local charge positioning during catalysis. In particular, the ααββ isomer being a factor of two faster than the αβαβ does not support the suggestion that a $CO_2^{\bullet-}$ ligand is *specifically* stabilized by cations on opposite sides of the porphyrin. This conclusion does not preclude the possibility that the *o*-$[N(CH_3)_3]^+$ groups improve individual thermodynamic steps during catalysis (e.g., CO_2 binding),[13,15] only that such changes have little effect on the overall kinetic profile or are balanced by unfavorable changes, such as the barrier for reaction from the stabilized intermediate. As conceptually described by the Sabatier Principle, comparing the rates of a complex, multi-step sequence often involves counterbalancing favorable and unfavorable changes in the reaction kinetics and thermodynamics of intermediates.[33-34]

B) Mechanistic insights

The mechanism of CO_2 reduction by Fe(*o*-TMA) is complex and does not follow the prototypical mechanism ascribed to CO_2RR by simple iron porphryins.[28-29,32] At lower phenol concentrations, 10-200 mM PhOH in DMF with 1 atm CO_2, the catalytic wave for the αβαβ isomer is observed only at *~0.3 V more negative* potentials than $E_{1/2}(Fe^I/Fe^0)$ (**Figure 7A**, **Figures S27-S30**). Under these conditions, the potential and reversibility of the iron(I/0) couple were almost completely unaffected. The loss of reversibility about the iron(II/I) couple indicates that turnover still results in CO, and background proton reduction occurs at even more negative potentials (**Figure S19**).

With increasing [PhOH], the reversibility of the iron(I/0) couple decreased, the irreversible current rose steeply, and the onset of catalysis moved to substantially more positive potentials. Above 1.0 M PhOH, the catalytic wave ultimately obscured $E_{1/2}(Fe^I/Fe^0)$, **Figure 7A**. The same behavior was also observed for the ααββ, αααβ, and αααα isomers. This behavior is unusual and contrasts the more common current-potential responses observed using iron tetraphenylporphyrin, Fe(TPP), and other neutral iron porphyrin catalysts (**Figure 7B**).[28-29,32] The typical behavior is characterized by the onset of catalysis at the potential of a catalyst redox couple, in this case at the $E_{1/2}$ for Fe^I/Fe^0. In addition, the potential of the catalytic wave in a prototypical CV response does not move significantly as substrate concentrations are added.

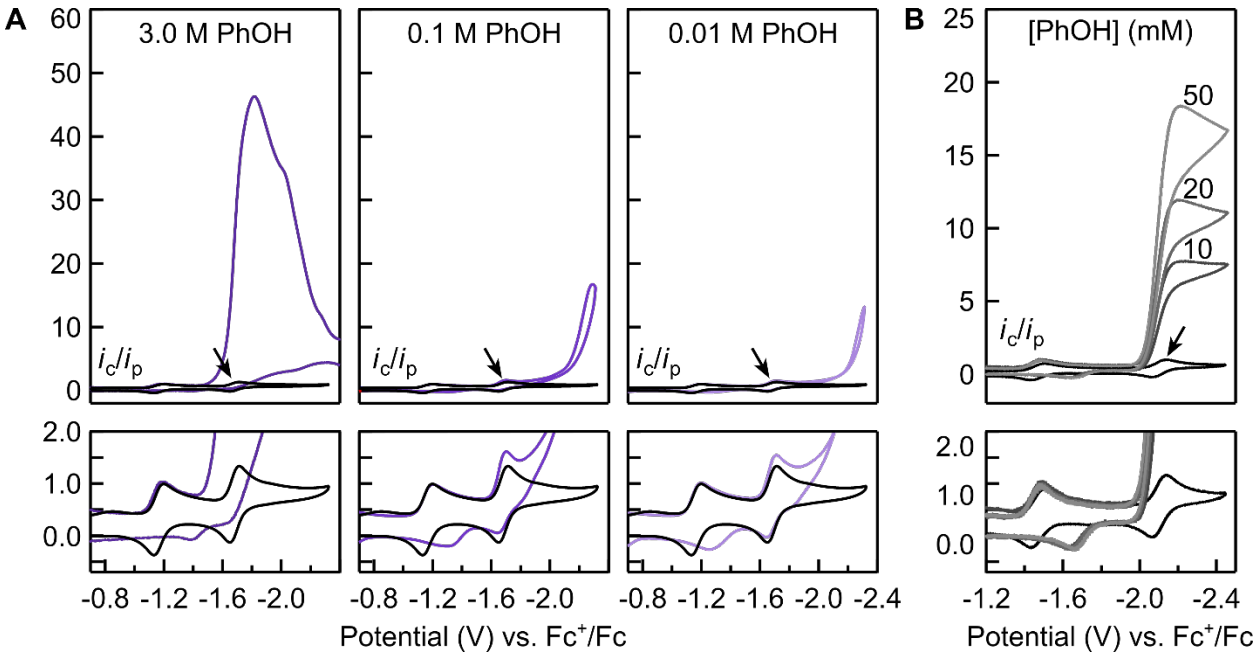

Figure 7. Cyclic voltammograms of CO_2 reduction at three different phenol concentrations by (**A**) αβαβ Fe(*o*-TMA) and (**B**) Fe(TPP). The top panels show the irreversible, catalytic currents with arrows that

indicate the Fe^{I}/Fe^{0} redox couple; the bottom panels have an expanded current scale to show the catalyst couples and the base of the catalytic wave. All currents were normalized to i_p values of the Fe^{II}/Fe^{I} couple. All data collected at 0.1 V s^{-1} in DMF containing 0.1 M [*n*-Bu_4N][PF_6], 0.1 M [H_2O], and 1.0 atm CO_2.

Taken together, the CV behavior for the Fe(*o*-TMA) atropisomers rules out the typical *E*C′ mechanism common to iron porphyrins that catalyze CO_2 reduction, where *E* is the Fe^{I}/Fe^{0} reduction and C′ is a composite set of pre-equilibria and turnover limiting steps. Rather, the data seem more consistent with an E_1CE_2C' reaction (where $E_1 > E_2$), **Scheme 3**.[35] In this mechanism, E_1 is an initial reduction event, C is some chemical step such as a pre-equilibrium or series of pre-equilibria, E_2 is the reduction of the product formed *in situ* following C, and C′ is the turnover limiting step (or series of steps). A version of this mechanism has been previously reported for CO_2 reduction by iron *o*,*o*-dihydroxyphenylporphyrin, for which E_1 corresponded to $E_{1/2}(Fe^{I}/Fe^{0})$, C represented pre-equilibrium CO_2 binding and protonation by PhOH, and E_2 was proposed to be coupled to C′ in a single, concerted electron transfer, proton transfer, and C-O bond breaking event.[28,36] We cannot rule out a possible change in mechanism as [PhOH] is increased; however, the overall shape of the voltammograms between 0.1 M and 3.0 M phenol does not sharply change and is good evidence for a common mechanism (**Figure S31**). We note that, while often convenient, FOWA cannot be applied to these voltammograms because the E_1C step(s) proceeding the catalytic wave obscures the 'foot' of the catalytic component (E_2C′).

Scheme 3. (**A**) Generalized electrochemical mechanism and effective overpotential definitions for an *E*C′ and E_1CE_2C' reaction, where $E_1 > E_2$. Nomenclature and labels match those in reference [35]. (**B**) Proposed mechanism described in the text. Boxed step(s) represent various solution equilibria and reduction step, following the same form as the square scheme shown in **Scheme 2**, above.

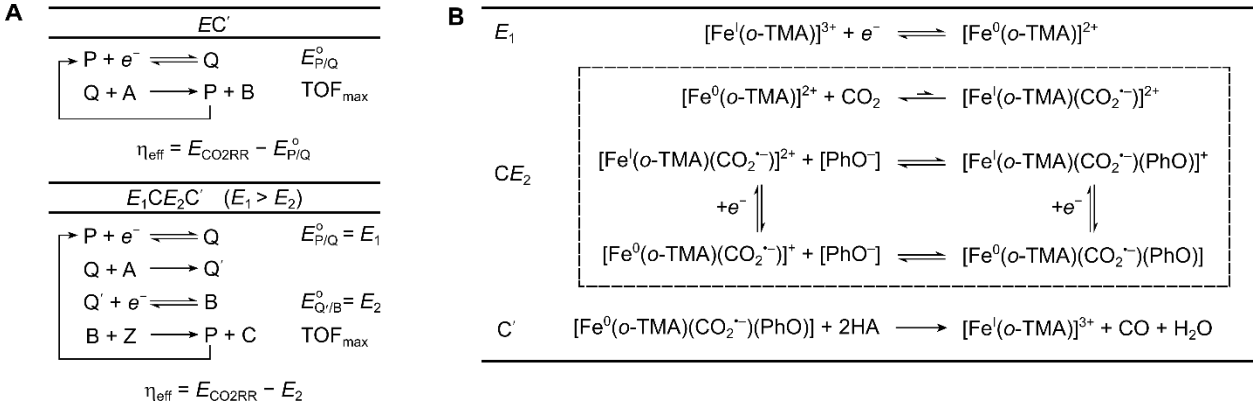

Identifying an E_1CE_2C' response has key mechanistic implications. Perhaps most significant is that catalysis does not occur at the Fe^{I}/Fe^{0} couple (P/Q, in **Scheme 3**). Rather, turnover only occurs after reducing a complex that is generated in-situ from the product of Fe^{0} and some solution species (Q′/B, in **Scheme 3**). The data do not give much insight into the chemical natures of the active catalysts Q′ and B, but some general conclusions can be made.

In the absence of PhOH, the Fe^{I}/Fe^{0} couple does not change under 1 atm CO_2. Making the typical assumption that the equilibrium constant of CO_2 binding to Fe^{I} is very small,[28] the lack of change in $E_{1/2}(Fe^{I}/Fe^{0})$ indicates that CO_2 binding to Fe^{0}—if occurring—is reversible and unfavorable at 20 °C. We note that while the equilibrium constant may be small, this does not preclude a forward rate constant for CO_2 binding that is sufficiently fast as to exceed the rate determining step. The change in catalytic onset potential with increasing concentrations of phenol suggests that E_2(Q′/B) is either (*i*) coupled to the rate-

determining chemical step, which must involve PhOH, or (*ii*) dependent on the concentration of PhOH/[PhO^-] in the reaction diffusion layer, as would be the case for [PhO^-] binding to either species Q′ or B. The former option is unlikely, given that the shift in the catalytic onset potential is >0.5 V from 0.1 to 3.0 M PhOH (**Figure 7A**) [for a reaction with a first order dependence on PhOH, a 30× increase in substrate would result in a shift of only ~0.05 V]. The latter option cannot be ruled out with the available data.

The need for very large concentrations of phenol and the high propensity of Fe(*o*-TMA) to bind anionic ligands leads us to speculate that the reduced, active catalyst Q′/B might bind trace phenoxide under these highly non-standard conditions. Such a model is shown in **Scheme 3B**, for which Q is $[Fe^0(o\text{-TMA})]^{2+}$, Q′ is $[Fe^I(o\text{-TMA})(CO_2^{\bullet-})(PhO)]^+$, and B is $[Fe^0(o\text{-TMA})(CO_2^{\bullet-})(PhO)]$. In this model, it is ~0.5 V more favorable to bind *both* CO_2 and PhO^- to the reduced form of the catalyst Q^{1-} than it is to bind both ligands to the oxidized form, Q. Similar parallelisms occur for O_2 reduction catalyzed by Fe(*o*-TMA) in acetate buffer, for which only the acetate-bound form of the Fe^{II} catalyst is active.[14] The large shift observed between 0.1 M and 3 M phenol concentrations could also in part reflect changes in the nature of the solvent, since (as noted above) the latter is ~0.24 mole fraction phenol.

While elucidating the detailed mechanistic pathway for CO_2RR is beyond the scope of this report, the clear dependence of E_2 on [PhOH] indicates that the mechanism is more complex than previously suggested.[13] This makes estimating the effective overpotential troublesome, as discussed in the next section.

C) Implications about the overpotential for CO_2 reduction.

For molecular electrocatalytic processes, the effective overpotential is usually defined as the difference between the equilibrium potential for the catalytic process under the reaction conditions (E_{CO2RR}) versus the half-wave potential of the catalytic wave ($E_{cat/2}$). For standard *EC′* electrocatalytic processes, such as in **Figure 7B**, the $E_{cat/2}$ occurs at the catalyst half-wave potential ($E_{1/2}$), in this case the $E_{1/2}(Fe^I/Fe^0)$. For an E_1CE_2C' reaction, however, $E_{cat/2}$ occurs at the E_2 potential, more specifically the $E_{Q'/B}$ in **Scheme 3**.[35] Note that—by definition—the value of $E_{Q'/B}$ is for a particular set of reaction conditions, defined here as 3.0 M PhOH, 1.0 atm CO_2, and 0.1 M H_2O. We confirmed that $E_{cat/2}$ occurs at $E_{Q'/B}$ following the methodology of Costentin and Savéant,[35] simulating the plateau-shaped voltammograms at 3.0 M PhOH and using the TOF_{max} values in **Table 3**. For these simulations, the potential at which half the plateau current is obtained ($E_{pl/2}$) is equal to $E_{Q'/B}$ (see SI, including **Figure S26**). We note that the *standard state* $E°_{Q'/B}$ would refer to a solution containing equal concentrations of PhO^- and PhOH, and with no changes to concentrations in the RDL during turnover. However, experimental limitations prohibited buffering of the solution, and the scope of the CO_2RR portion of this work is limited to the conditions under which Fe(*o*-TMA) was originally analyzed (e.g. no buffer).[13] Thus, in defining $E_{Q'/B}$, we have to assume that some concentration of PhO^- is present in the RDL as a result of turnover and that this concentration is relatively constant for the four atropisomers. This assumption is fairly good, as the four atropisomers all have similar TOF_{max} values and are likely to yield similar amounts of PhO^- during the forward sweep. The four atropisomers have $E_{Q'/B}$ values that are very close to each other, within the error of the estimation (average $E_{Q'/B}$ = 1.84 ± 0.04 V, **Table 3**). The value of E_{CO2RR} has been estimated under these conditions as −1.43 V vs. Fc^+/Fc.[13] This estimated value uses the unusual standard state of 1 M CO_2 and using pK_a values and the Henry's law constant for CO_2 in DMF for these non-standard conditions of ~0.76/0.24 mol fraction DMF/PhOH with 0.1 H_2O and 0.1 M ionic strength.

The values for η_{eff} were estimated for the set of atropisomers and are reported in **Table 3**. The range in these estimates is small, with the αβαβ, ααββ and αααβ having $\eta_{eff} \geq 0.39$, 0.39 and 0.37 V, and the αααα being higher, ≥ 0.48 V. More accurate values could not be obtained from the voltammetry due to the fitting method (see SI). The similarity in η_{eff} values was expected because the atropisomers have nearly the same $E_{Q'/B}$ (i.e., E_2) values and were studied under the same conditions. The average η_{eff} for CO_2 reduction by the

Fe(*o*-TMA) atropisomers is $\eta_{eff} \geq 0.41$ V, at least 0.19 V larger than the value reported by Savéant et al.[13] Even with this correction, the TOF_{max} and overpotential metrics for Fe(*o*-TMA) are still among the best molecular catalysts for CO_2 reduction, similar to the metrics reported by these researchers for the iron *o*,*o*-dihydroxyphenylporphyrin electrocatalyst.[37]

D) CO_2 Reduction Conclusions

Three important conclusions are evident from these CO_2 studies:

i. All four atropisomers of Fe(*o*-TMA) perform the CO_2RR with fast rates and low overpotentials and are largely indistinguishable. The largest difference in TOF_{max} is only a factor of 5, and the estimated overpotentials are all within 0.1 V. Thus, the orientations of the four cationic *o*-$[N(CH_3)_3]^+$ groups do not significantly influence the effectiveness of these isomers as CO_2RR electrocatalysts. This argues against a specific cation geometry for stabilizing a particular intermediate. The cationic charges are certainly important, as these catalysts have exceptional metrics for the CO_2RR under these peculiar conditions. *The impact of the o-$[N(CH_3)_3]^+$ groups comes from the total charge on the catalyst, not the orientation of charges.*

ii. The voltammograms of CO_2 reduction by Fe(*o*-TMA) do not support an *E*C′ mechanism. Rather, they are more consistent with an E_1CE_2C' mechanism in which $[Fe^0(o\text{-TMA})]^{2+}$ is not involved in the rate-determining step. Turnover is instead defined by a follow-up reduction and chemical steps. The potential of this further-reduced species is strongly dependent on the concentration of PhOH in solution, suggesting some pre-equilibrium between the active catalyst and PhOH/$[PhO^-]$ in solution. The conclusion of an E_1CE_2C' mechanism also requires a revision of the estimated overpotentials η_{eff}. We conservatively estimate $\eta_{eff} \geq 0.41$ V under these conditions, which is 0.19 V larger than the overpotentials originally reported.[13] Given that the η_{eff} values are approximately the same within the set of isomers, it is perhaps unsurprising that the isomers also have similar TOF_{max} values.

iii. The data presented in this study allow us to parse the contributions of the individual atropisomers to the electrocatalysis reported in reference [14] and [13]. From repeating the reported synthesis, we estimated that the prior studies used a mixture of the Fe(*o*-TMA) atropisomers containing ca. 40% each of the αβαβ and αααβ isomers, ca. 15% of the ααββ, and 5% of the αααα.[18] Using these populations and assuming that the catalysts act independently in a mixed solution, more than 80% of the ORR catalysis reported in reference [14] was due to the αβαβ isomer. This is due to its highest concentration and highest TOF_{max}. In contrast, the data reported by Savéant *et al* for the CO_2RR in reference 13 includes substantial contributions from all four species: αβαβ, 20%; ααββ, 20%; αααβ, 50%; αααα, 10%.

Conclusions from ORR and CO_2RR studies considered together

The polycationic Fe(*o*-TMA) system is an exceptional electrocatalyst for the reduction of both O_2 and CO_2, as previously shown using mixtures of the four atropisomeric forms. Using isolated samples of each atropisomer, the studies here show that each is an excellent catalyst. Their catalytic properties vary only modestly with the positioning of the positive charges, from two-on-each-side of the porphyrin ring (αβαβ and ααββ) to one that bears all four charges on the same side (αααα). The ORR catalysis shows the larger variation, with the αβαβ isomer being 60 times faster than the αααα isomer. For CO_2RR under the reported conditions, the difference between the isomers is less than a factor of 5. CO_2RR utilizes much more reduced iron centers, and the rate order between the atropisomers is mostly reversed, with the αααα isomer being the fastest. In contrast, prior results using the *para*-isomer show much slower rates and higher overpotentials than any of the series studied in this work. These results show that *the primary catalytic benefits of the o-TMA^{4+} ligand come from its high overall charge near the metal center, not the oriented positioning of the individual charges*. Thus, the electric field or potential radiating out from the polycationic catalyst has a

much larger influence than the local field at the iron center, which should be much larger in the C_{4v} αααα isomer than in the D_{2d} and C_{2h} αβαβ and ααββ isomers.

The variation in the ORR turnover frequencies closely parallel the $E_{1/2}$ and overpotential values of the atropisomers under catalytic conditions. The αβαβ isomer is the fastest and has an overpotential that is 49 mV larger than the slowest, αααα isomer. This is qualitatively in-line with prior studies of the ORR that showed correlations between TOF_{max} and η_{eff}.[19,22] For CO_2RR, the catalytic system with the highest η_{eff}, αααα, is again the fastest, though this pattern is not monotonic (perhaps because of the small ranges of TOF_{max} and η_{eff}).

The variations in TOF_{max} and η_{eff} in the ORR catalysis results from the different catalyst $E_{1/2}(Fe^{III}/Fe^{II})$ values under catalytic conditions. The $E_{1/2}(Fe^{III}/Fe^{II})$ values of the isomers are different because of relative differences in acetate binding to the ferric and ferrous forms of Fe(*o*-TMA), with larger $K_{AcO}(Fe^{III})$: $K_{AcO}(Fe^{II})$ ratios resulting in more negative $E_{1/2}(Fe^{III}/Fe^{II})$ values. These directly measured binding constants are very different between the ferric and ferrous complexes, but the differences between the atropisomers are smaller, within a factor of 4 in both series. Thus, again, the positioning of the cationic charges plays a more minor role than the overall charge of the porphyrin ligand.

The CO_2RR cyclic voltammograms for the individual atropisomers shows that the catalysis is more complicated than the *EC′* mechanism previously suggested. Rather, an E_1CE_2C' mechanism is more consistent with the data. The data show that the $[Fe^0(o\text{-TMA})]^{2+}$ species, previously thought to be the species that binds CO_2, does not define catalytic turnover. Instead, catalysis requires more negative potentials than is needed to generate that species. The mechanistic re-evaluation also indicates a higher overpotential for the CO_2-to-CO catalysis than was previously reported.

There are two major take-aways from this work that should be an important guide to catalyst design. (*i*) High cationic charge close to the metal active site can have a very large effect on the energetics and kinetics, but (*ii*) the relative positioning of the cationic charges has only a small effect. The charges seem to affect catalysis in large part indirectly, by enhancing ligand binding to change the nature of the catalytic species.

Supporting Information

The supporting information file contains the complete set of electrochemical and UV-visible data, simulated curves, and mathematical derivations described in the text. In addition to these data, this file also contains a complete list of materials and methods used to prepare the molecules and perform the measurements described in this study.

Acknowledgement

This work was supported as part of the Center for Molecular Electrocatalysis (CME), an Energy Frontier Research Center funded by the U.S. Department of Energy, Office of Science, Basic Energy Sciences. D.J.M. acknowledges a graduate fellowship from the U.S. National Science Foundation.

References

1. Fried, S. D.; Boxer, S. G., Electric Fields and Enzyme Catalysis. *Annu. Rev. Biochem* **2017,** *86* (1), 387-415.
2. Shaik, S.; Mandal, D.; Ramanan, R., Oriented electric fields as future smart reagents in chemistry. *Nat. Chem.* **2016,** *8* (12), 1091-1098.

3. Xiang, L.; Tao, N. J., Organic chemistry: Reactions triggered electrically. *Nature* **2016,** *531* (7592), 38-39.
4. Cammarota, R. C.; Lu, C. C., Tuning Nickel with Lewis Acidic Group 13 Metalloligands for Catalytic Olefin Hydrogenation. *J. Am. Chem. Soc.* **2015,** *137* (39), 12486-9.
5. Chantarojsiri, T.; Reath, A. H.; Yang, J. Y., Cationic Charges Leading to an Inverse Free-Energy Relationship for N-N Bond Formation by Mn(VI) Nitrides. *Angew. Chem. Int. Ed. Engl.* **2018,** *57* (43), 14037-14042.
6. Chantarojsiri, T.; Ziller, J. W.; Yang, J. Y., Incorporation of redox-inactive cations promotes iron catalyzed aerobic C–H oxidation at mild potentials. *Chem. Sci.* **2018,** *9* (9), 2567-2574.
7. Ciampi, S.; Darwish, N.; Aitken, H. M.; Díez-Pérez, I.; Coote, M. L., Harnessing electrostatic catalysis in single molecule, electrochemical and chemical systems: a rapidly growing experimental tool box. *Chem. Soc. Rev.* **2018,** *47* (14), 5146-5164.
8. Kang, K.; Fuller, J., 3rd; Reath, A. H.; Ziller, J. W.; Alexandrova, A. N.; Yang, J. Y., Installation of internal electric fields by non-redox active cations in transition metal complexes. *Chem. Sci.* **2019,** *10* (43), 10135-10142.
9. Margarit, C. G.; Asimow, N. G.; Gonzalez, M. I.; Nocera, D. G., Double Hangman Iron Porphyrin and the Effect of Electrostatic Nonbonding Interactions on Carbon Dioxide Reduction. *J. Phys. Chem. Lett.* **2020,** *11* (5), 1890-1895.
10. Rao, H.; Schmidt, L. C.; Bonin, J.; Robert, M., Visible-light-driven methane formation from CO_2 with a molecular iron catalyst. *Nature* **2017,** *548* (7665), 74-77.
11. Tsui, E. Y.; Tran, R.; Yano, J.; Agapie, T., Redox-inactive metals modulate the reduction potential in heterometallic manganese-oxido clusters. *Nat. Chem.* **2013,** *5* (4), 293-9.
12. Ramirez, B. L.; Lu, C. C., Rare-Earth Supported Nickel Catalysts for Alkyne Semihydrogenation: Chemo- and Regioselectivity Impacted by the Lewis Acidity and Size of the Support. *J. Am. Chem. Soc.* **2020,** *142* (11), 5396-5407.
13. Azcarate, I.; Costentin, C.; Robert, M.; Savéant, J. M., Through-Space Charge Interaction Substituent Effects in Molecular Catalysis Leading to the Design of the Most Efficient Catalyst of CO_2-to-CO Electrochemical Conversion. *J. Am. Chem. Soc.* **2016,** *138* (51), 16639-16644.
14. Martin, D. J.; Mercado, B. Q.; Mayer, J. M., Combining scaling relationships overcomes rate versus overpotential trade-offs in O_2 molecular electrocatalysis. *Sci. Adv.* **2020,** *6* (11), eaaz3318.
15. Martin, D. J.; Johnson, S. I.; Mercado, B. Q.; Raugei, S.; Mayer, J. M., Intramolecular Electrostatic Effects on O_2, CO_2, and Acetate Binding to a Cationic Iron Porphyrin. *Inorg. Chem.* **2020,** *59* (23), 17402-17414.
16. Zhang, R.; Warren, J. J., Controlling the Oxygen Reduction Selectivity of Asymmetric Cobalt Porphyrins by Using Local Electrostatic Interactions. *J. Am. Chem. Soc.* **2020,** *142* (31), 13426-13434.
17. Mao, Y.; Loipersberger, M.; Kron, K. J.; Derrick, J. S.; Chang, C. J.; Sharada, S. M.; Head-Gordon, M., Consistent inclusion of continuum solvation in energy decomposition analysis: theory and application to molecular CO_2 reduction catalysts. *Chem. Sci.* **2021,** *12* (4), 1398-1414.
18. Martin, D. J.; Wise, C. F.; Pegis, M. L.; Mayer, J. M., Developing Scaling Relationships for Molecular Electrocatalysis through Studies of Fe-Porphyrin-Catalyzed O_2 Reduction. *Acc. Chem. Res.* **2020,** *53* (5), 1056-1065.
19. Pegis, M. L.; McKeown, B. A.; Kumar, N.; Lang, K.; Wasylenko, D. J.; Zhang, X. P.; Raugei, S.; Mayer, J. M., Homogenous Electrocatalytic Oxygen Reduction Rates Correlate with Reaction Overpotential in Acidic Organic Solutions. *ACS Cent. Sci.* **2016,** *2* (11), 850-856.
20. Martin, D. J.; Mercado, B. Q.; Mayer, J. M., All Four Atropisomers of Iron(III) and Iron(II) Tetra(*o*-*N*,*N*,*N*-trimethylanilinium)porphyrin. *Inorg. Chem.* **2021,** *60*, 5240-5251.
21. Elgrishi, N.; Rountree, K. J.; McCarthy, B. D.; Rountree, E. S.; Eisenhart, T. T.; Dempsey, J. L., A Practical Beginner's Guide to Cyclic Voltammetry. *J. Chem. Educ.* **2018,** *95* (2), 197-206.
22. Pegis, M. L.; Wise, C. F.; Koronkiewicz, B.; Mayer, J. M., Identifying and Breaking Scaling Relations in Molecular Catalysis of Electrochemical Reactions. *J. Am. Chem. Soc.* **2017,** *139* (32), 11000-11003.

23. Costentin, C.; Drouet, S.; Robert, M.; Savéant, J.-M., Turnover Numbers, Turnover Frequencies, and Overpotential in Molecular Catalysis of Electrochemical Reactions. Cyclic Voltammetry and Preparative-Scale Electrolysis. *J. Am. Chem. Soc.* **2012,** *134* (27), 11235-11242.
24. Rountree, E. S.; McCarthy, B. D.; Eisenhart, T. T.; Dempsey, J. L., Evaluation of Homogeneous Electrocatalysts by Cyclic Voltammetry. *Inorg. Chem.* **2014,** *53* (19), 9983-10002.
25. Pegis, M. L.; Martin, D. J.; Wise, C. F.; Brezny, A. C.; Johnson, S. I.; Johnson, L. E.; Kumar, N.; Raugei, S.; Mayer, J. M., Mechanism of Catalytic O_2 Reduction by Iron Tetraphenylporphyrin. *J. Am. Chem. Soc.* **2019,** *141*, 8315-8326.
26. Wulfsberg, G., *Principles of Descriptive Inorganic Chemistry*. Brooks/Cole: Monterey, CA, 1987.
27. McCarthy, B. D.; Martin, D. J.; Rountree, E. S.; Ullman, A. C.; Dempsey, J. L., Electrochemical reduction of brønsted acids by glassy carbon in acetonitrile-implications for electrocatalytic hydrogen evolution. *Inorg. Chem.* **2014,** *53* (16), 8350-61.
28. Costentin, C.; Robert, M.; Savéant, J. M., Current Issues in Molecular Catalysis Illustrated by Iron Porphyrins as Catalysts of the CO_2-to-CO Electrochemical Conversion. *Acc. Chem. Res.* **2015,** *48* (12), 2996-3006.
29. Saveant, J. M., Molecular catalysis of electrochemical reactions. Mechanistic aspects. *Chem. Rev.* **2008,** *108* (7), 2348-78.
30. Balducci, G.; Chottard, G.; Gueutin, C.; Lexa, D.; Saveant, J.-M., Electrochemistry of iron(I) porphyrins in the presence of carbon monoxide. Comparison with zinc porphyrins. *Inorg. Chem.* **1994,** *33* (9), 1972-1978.
31. Croisy, A.; Lexa, D.; Momenteau, M.; Saveant, J. M., Integrated molecular systems. Fixation of carbon monoxide on iron(I) in simple and superstructured porphyrins. *Organometallics* **1985,** *4* (9), 1574-1579.
32. Azcarate, I.; Costentin, C.; Robert, M.; Savéant, J.-M., Dissection of Electronic Substituent Effects in Multielectron–Multistep Molecular Catalysis. Electrochemical CO2-to-CO Conversion Catalyzed by Iron Porphyrins. *J. Phys. Chem. C* **2016,** *120* (51), 28951-28960.
33. Stegelmann, C.; Andreasen, A.; Campbell, C. T., Degree of rate control: how much the energies of intermediates and transition states control rates. *J. Am. Chem. Soc.* **2009,** *131* (23), 8077-82.
34. Kozuch, S.; Shaik, S., Kinetic-quantum chemical model for catalytic cycles: the Haber-Bosch process and the effect of reagent concentration. *J. Phys. Chem. A* **2008,** *112* (26), 6032-41.
35. Costentin, C.; Savéant, J.-M., Multielectron, Multistep Molecular Catalysis of Electrochemical Reactions: Benchmarking of Homogeneous Catalysts. *ChemElectroChem* **2014,** *1* (7), 1226-1236.
36. Costentin, C.; Passard, G.; Robert, M.; Saveant, J. M., Pendant acid-base groups in molecular catalysts: H-bond promoters or proton relays? Mechanisms of the conversion of CO_2 to CO by electrogenerated iron(0)porphyrins bearing prepositioned phenol functionalities. *J. Am. Chem. Soc.* **2014,** *136* (33), 11821-9.
37. Costentin, C.; Drouet, S.; Robert, M.; Savéant, J.-M., A local proton source enhances CO_2 electroreduction to CO by a molecular Fe catalyst. *Science* **2012,** *338*, 90-94.

For Table of Contents Only: